Room Temperature Synthesis of Bismuth Oxyiodide with Different Morphologies for the Photocatalytic Degradation of Norfloxacin

Saifullahi Shehu Imam[a]*, Zakariyya Uba Zango[b], Haruna Abdullahi[c]

[a]*Department of Pure and Industrial Chemistry, Bayero University, P.M.B 3011, Kano, Nigeria*

[b]*Department of Chemistry, Al-Qalam University Katsina, P.M.B 2341, Katsina, Nigeria*

[c]*Department of Applied Chemistry, Federal University Dutsinma, P.M.B 5001, Katsina, Nigeria*

[a]*Email: saifaz2005@gmail.com*

Abstract

In this study, both BiOI spheres and BiOI plates were synthesized successfully at room temperature and applied for the photocatalytic degradation of norfloxacin using indoor fluorescent light illumination. The samples were characterized by X-ray diffraction (XRD), Fourier transform infrared spectroscopy (FTIR), UV-Vis absorption spectrum, scanning electron microscope (SEM) and Brunauer-Emmett-Teller (BET). Although both BiOI spheres and BiOI plates displayed approximately similar absorption band edge, higher photocatalytic degradation was noticed in the case of BiOI spheres as compared with BiOI plates. This was attributed to the unique features of BiOI spheres, such as enlarged specific surface area and enhanced adsorption capacity. The study demonstrated that morphology has a key role in improving the degradation efficiency of a photocatalyst.

Keywords: Photocatalytic degradation; Room-temperature synthesis; BiOI spheres; BiOI Plates; Norfloxacin.

1 Introduction

Annual worldwide consumption of fluoroquinolones stands around 44 million kilograms [1]. Among the fluoroquinolones, norfloxacin antibiotic is a frequent prescribed medication for both human and veterinary purpose, as it acts against both gram positive and gram negative bacteria [2]. After ingestion, more than 50% of norfloxacin is excreted unaltered, this leads to its frequent detection in water bodies, for example, in hospital wastewater alone, concentrations of over 100 μgL^{-1} have been reported [3-5].

----

* Corresponding author.

Its presence has serious repercussions, as apart from polluting the water thereby resulting in intense and perpetual lethality, it enhance the development of antibiotic-resistant bacteria [6]. Since conventional treatment methods hardly remove pharmaceuticals from wastewater to the levels required by law, the development of more effective treatment technologies becomes imperative [7]. Many techniques such as adsorption [8], micro-extraction [9], electrochemical oxidation [10], combined photo-Fenton and biological oxidation [11], aerobic degradation [12], nanofiltration membranes [13], ozonation [14] and advanced oxidation processes (AOPs) [15] are now being employed for the destruction of organic pollutants. Among the advanced oxidation processes (AOPs), heterogeneous photocatalysis receives much attention specifically because of its unique properties of being promising and efficient as it converts harmful organic pollutants into safer end products [16]. Infact, its capability at room temperature and pressure have been widely demonstrated. However, the major challenge now is the inadequate number of visible light responsive photocatalysts which represents over 40% of the solar radiation [17]. Bismuth-based compounds such as $BiVO_4$ [18], Bi_2S_3 [19], Bi_2WO_6 [20], Bi_2O_3 [21], $Bi_4Ti_3O_{12}$ [22], Bi_2MoO_6 [23], $Bi_2O_2CO_3$ [24] and BiOX (X= Cl, Br, I) [25-27] have recently received much attention, as they are able to degrade organic pollutants using visible light radiation. Among the bismuth-based compounds, high emphasis is been placed on the BiOX (X=Cl, Br, I) family, mainly because of their unique structure constructed by interleaved $[Bi_2O_2]^{2+}$ slabs and $[X]^{2-}$ slabs (X=Cl, Br, I), resulting in the formation of internal electric fields, which obviously facilitates the separation of photogenerated electrons and holes [28-30]. Compared to BiOBr or BiOCl, preference is given to BiOI for its narrow band gap and strong absorption in the visible region. Preparation methods such as hydrothermal [31], solvothermal [32] and soon are commonly employed for the synthesis of BiOX (X=Cl, Br, I), but are tedious, operated at elevated temperature and pressure and are often complicated [33].

The objective of this study is to synthesize BiOI catalysts with different morphologies via room temperature synthesis, characterize them using FTIR, SEM, TEM, BET, UV-Vis absorption spectrum and XRD before finally evaluating their photocatalytic performance on the degradation of norfloxacin using indoor fluorescent light illumination.

2 Materials and Methods

2.1 Chemicals

All chemicals used were of analytical grade and used without further treatment. Bismuth nitrate pentahydrate $(Bi(NO_3)_3.5H_2O)$, Potassium iodide (KI) and Absolute ethanol were supplied by QReC Chemicals, while Polyethylene glycol (PEG400) was supplied by Merck Germany and norfloxacin by Sigma Aldrich respectively.

2.2 Preparation of BiOI Catalysts

2.2.1   Preparation of BiOI Spheres

5 mmol of $Bi(NO_3)_3.5H_2O$ were grounded continuously for 5 mins using an agate mortar to ensure evenness, 3 ml of PEG400 was then added, and grinding continues for further 5 mins. Subsequently, 5 mmol of KI were added and grounded together for 20 mins. After that, the product was washed several times with distilled water

and then with absolute ethanol before dried in an oven at 80 ^{o}C [34].

2.2.2   Preparation of BiOI Plates

2 mmol of Bi(NO$_3$)$_3$.5H$_2$O and 2 mmol of KI were mixed thoroughly and grounded resulting in the formation of black paste. 5 ml of distilled water was then added and mixed well with the black paste. This was subsequently allowed to stand at room temperature for 3 hrs. After that, the product was washed several times with distilled water and then with absolute ethanol before dried in an oven at 80 ^{o}C [35].
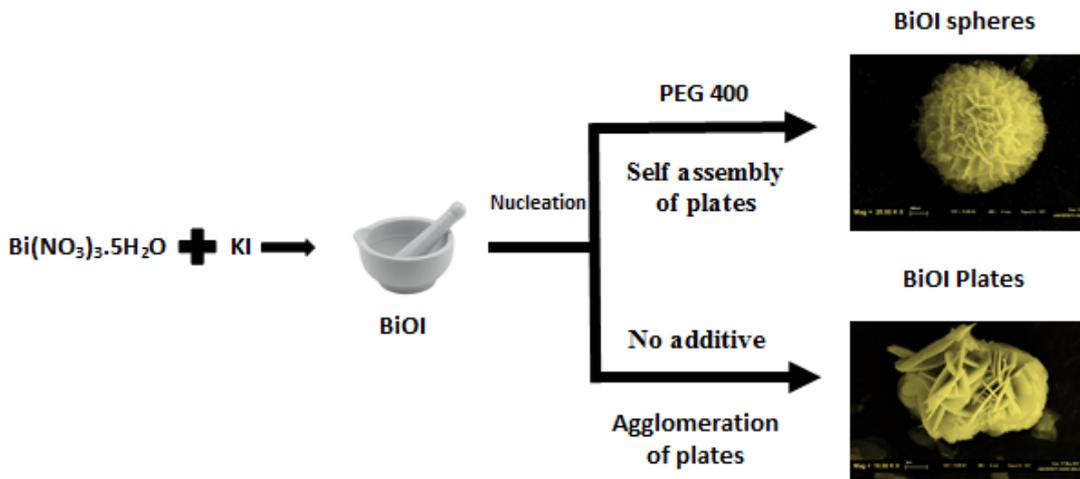

Figure 1: Possible growth mechanism of BiOI spheres and BiOI plates

Based on the above schematic representation, the reaction that occurred in the formation of BiOI may be explained by equation (1) below:

$$Bi(NO_3)_3.5H_2O + KI \rightarrow BiOI \downarrow + 2HNO_3 + KNO_3 + 4H_2O \qquad (1)$$

2.3   Photocatalytic Experiment

Photocatalytic activity was evaluated using norfloxacin as a model pollutant. Different norfloxacin concentrations (10 – 100 mg/L) were prepared using the stock solution. The suspensions were subsequently prepared by adding variable amounts (0.5 – 2 g) of the photocatalyst powder per liter of norfloxacin solution. The photocatalytic reactions were carried out at room temperature in a 500 mL pyrex beaker using indoor fluorescent light illumination and maintaining eco living day light fluorescent (25 W) as the source throughout. Prior to irradiation, the suspensions were stirred in the dark using a magnetic stirrer for 30 mins to reach adsorption-desorption equilibrium. Periodically after irradiation, 5 mL of the suspension was taken out using a syringe and centrifuged for 5 mins at 4000 rpm essentially to remove the catalyst from the norfloxacin suspension and then filtered. Concentration of the filtrate was subsequently analyzed at 273 nm (λ_{max}) using a UV-Vis spectrophotometer (Shimadzu 2600). All experiments were conducted in duplicates and at the inherent solution pH which remain unaltered during irradiations. The photodegradation efficiency (η) was calculated by the following equation:

$$\eta \ (\%) = \frac{C_o - C_t}{C_o} \times 100 \qquad (2)$$

Where C_o is the initial concentration and C_t is the concentration at time (t) respectively.

3   Results and Discussions

3.1   Characterization Results

3.1.1   XRD Analysis

The crystal structure of both BiOI spheres and BiOI plates were analyzed by X-ray diffraction (XRD), no impurity peaks were detected, which indicates that pure BiOI was successfully synthesized using both routes. As shown in Fig. 1, all diffraction peaks from both BiOI spheres and BiOI plates can well be indexed to (002), (101), (102), (110), (111), (103), (004), (200), (114), (212), (213), (204) and (220) planes of the tetragonal phase of BiOI. The results were in good agreement with the results of XRD patterns of BiOI reported by JCPDS (file no. 73.2062) for samples synthesized in the presence of KI. However, the intense and sharp diffraction peaks of BiOI spheres indicates the high crystallization of the BiOI spheres.
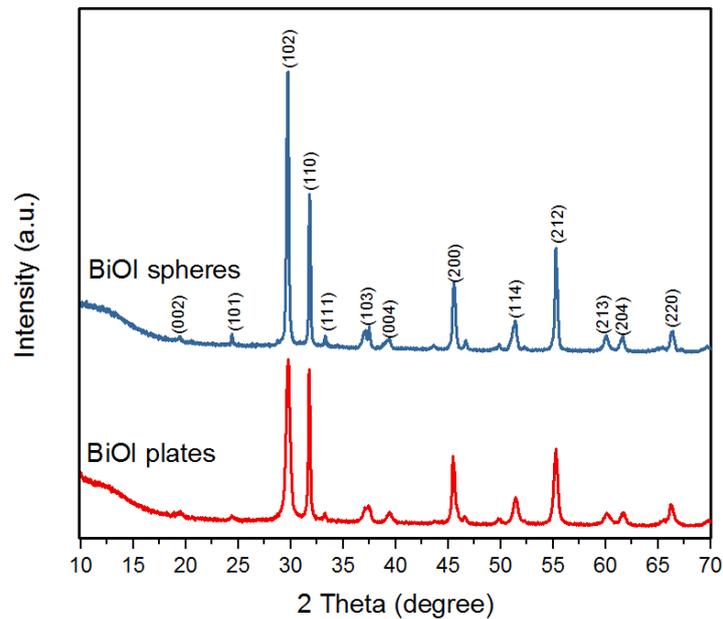

Figure2: XRD pattern of as-synthesized BiOI spheres and plates.

3.1.2   FTIR Analysis

Fourier transform infrared spectroscopy (FTIR) analysis was conducted for dual purposes. First was to determine the surface functional groups and second was to confirm the complete eradication of PEG400 from the surface of BiOI spheres. As shown in Fig. 2, the absorption peaks of BiOI spheres and BiOI plates are almost identical. Both spectra have peaks at low frequency around 500 cm^{-1} which are assigned to Bi – O

29

vibration of chemical bonds in BiOI [36]. Absorption peaks at around 1045 cm^{-1} may be assigned to asymmetric stretching vibration peaks of Bi – I band in BiOI structure, while absorption peaks at 1650 cm^{-1} are the H – O – H of physical adsorbed water [37]. Broad absorption peaks at 3450 cm^{-1} are due to the O – H stretching vibration over the samples [38].
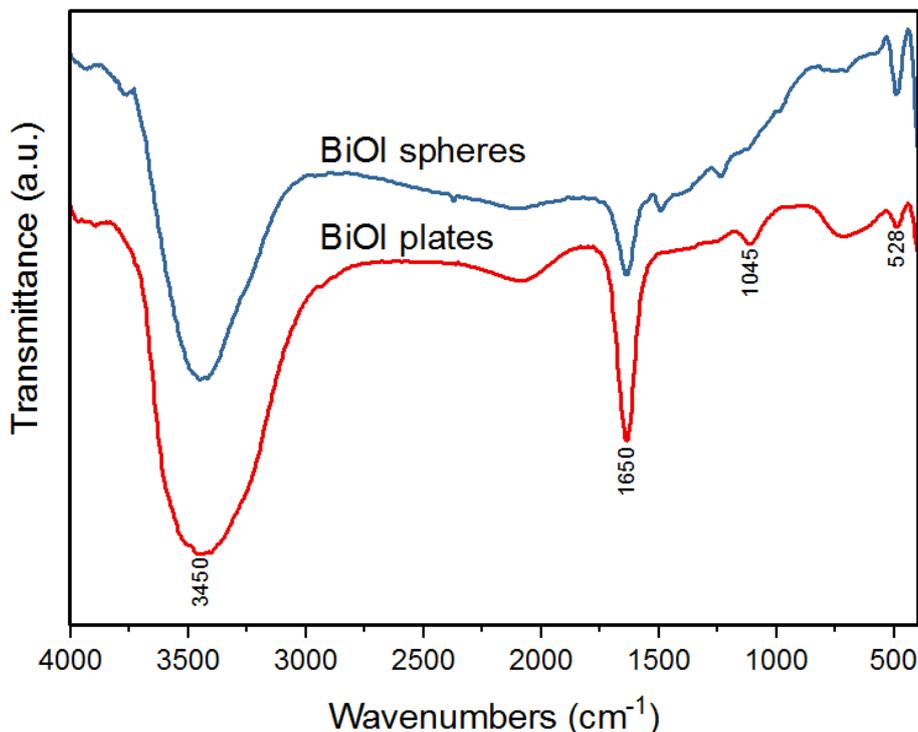

Figure 3: FTIR spectra of as-synthesized BiOI spheres and plates.

3.1.3   SEM Analysis

Since solvents with different viscosity were used in the synthesis of BiOI. This would have direct impact on its morphology, basically solvent of low viscosity facilities high diffusion rate of ions, while high viscosity solvent slows the diffusion rate of ions.

Morphologies of the as-synthesized BiOI catalysts were first examined by SEM (Fig. 3). Low magnification images show that the BiOI catalysts have spherical-like shape (Fig. 3a) and plate-like shape (Fig. 3d).

This served as a first stage confirmation of the unique role of PEG 400 in the synthesis of BiOI spheres, It has prevented the agglomeration of plates (Fig. 3f) and resulted in a self-assembly of numerous plates, loosely packed and intercrossed each other (Fig 3c).

3.1.4   UV – Vis Absorption Spectrum

UV – Vis absorption spectrum analysis was also conducted for dual reasons. First was to determine the band gaps of both BiOI spheres and BiOI plates, second is to confirm that BiOI spheres has no added advantage over

BiOI plates in terms of optical absorption. It can be observed from Fig. 4 that both synthesized samples showed noticeable absorption at wavelength close to 700 nm, with an absorption edge of 675 nm and 668 nm for BiOI spheres and BiOI plates respectively. The band gap energies (E_{bg}, eV) of the prepared samples were estimated using the following equation:

$$\lambda = \frac{1240}{E_{bg}} \qquad (3)$$

Based on the above equation, the band gap energies for BiOI spheres and BiOI plates were calculated to be 1.835 eV and 1.856 eV, which are close to the values reported in literature [39]. From the calculated band gap energies, it is clear that the synthesized BiOI samples were theoretically feasible for photocatalytic degradation of organic pollutants under visible light radiation.
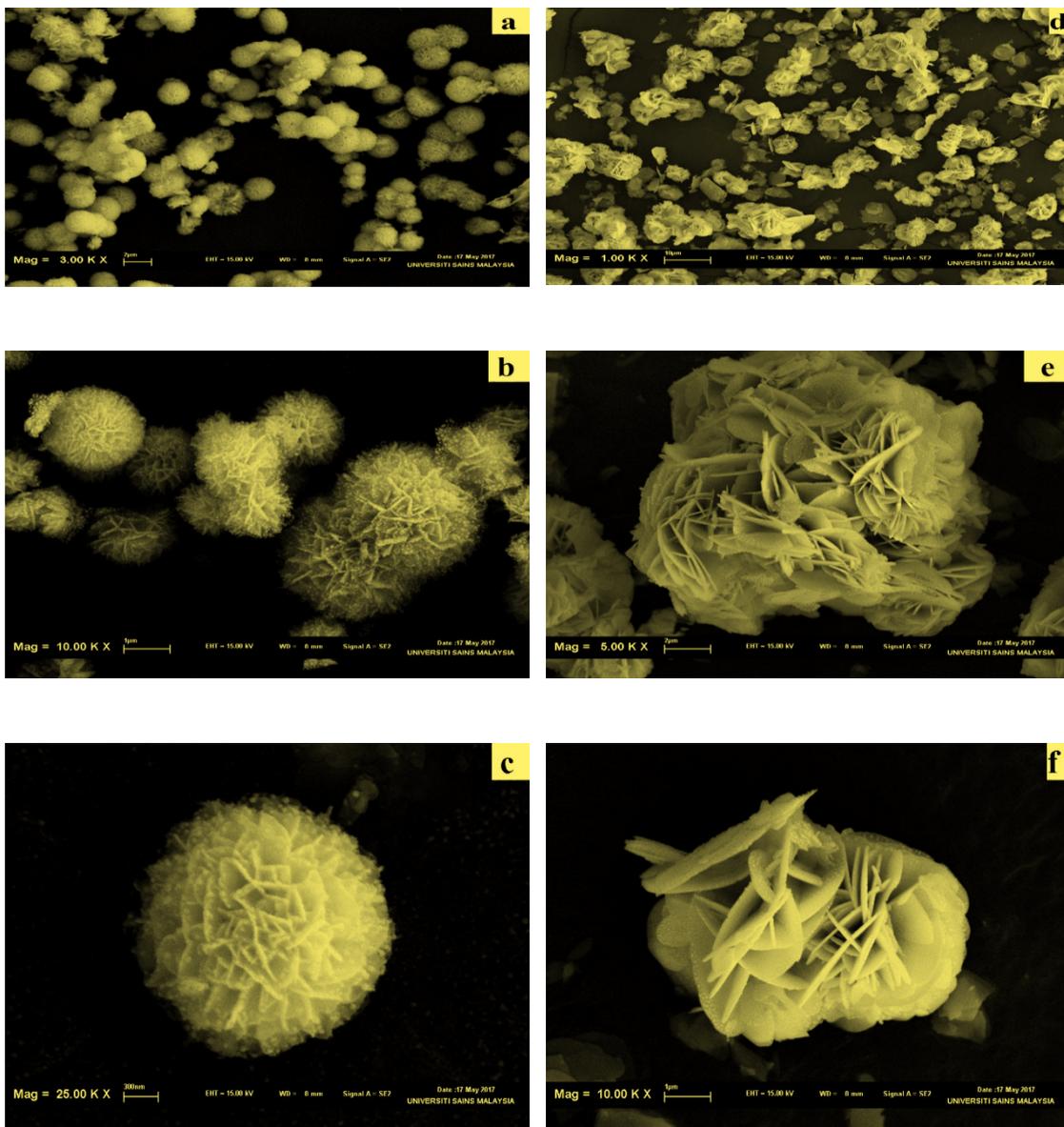

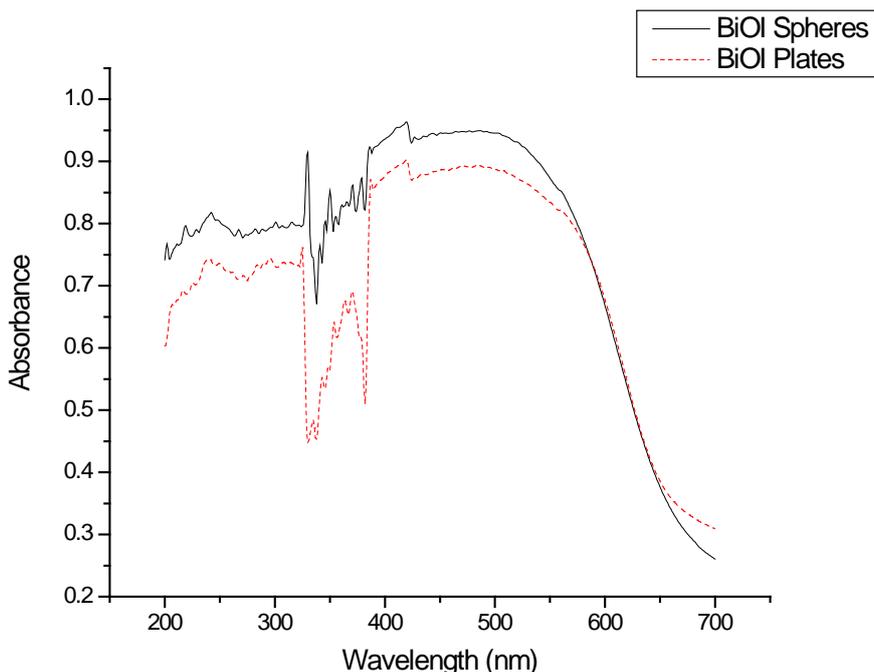**Figure 4:** SEM images of the as-synthesized BiOI spheres (a,b,c) and BiOI plates (d,e,f).

Figure 5: UV-Vis absorption spectrum of BiOI spheres and BiOI plates.

3.1.5   BET Analysis

A vital factor that affects the photocatalytic ability of a semiconductor is its surface area, as semiconductors with larger specific surface areas displayed much better efficiency in their performance.

This is because larger surface area may favour the adsorption of more effluents onto the surface of the semiconductor, which in turn facilitates photocatalytic activity [40]. In view of the above importance, surface areas of both BiOI spheres and BiOI plates were determined. Fig. 5 below is the nitrogen adsorption-desorption isotherm and Barret-Joyner-Halender (BJH) pore size distribution curves.

The isotherms according to IUPAC classification corresponds to type IV with BiOI spheres having a H3 hysteresis loop, a common feature of mesoporous solids, while BiOI plates lacks hysteresis loop, a common feature of non-porous solids. In line with that, the pore size distribution curves also reveals that BiOI spheres have a mesoporous structure, while BiOI plates is nearly non porous.

The BET specific surface areas (A_{BET}) of BiOI spheres and BiOI plates were calculated to be 16.05 m^2/g and 4.99 m^2/g, an indication that the surface area of the former is more than three times larger than the later. Based on the above observations, BiOI spheres is expected to have higher adsorption capacity and photocatalytic activity for the degradation of norfloxacin.
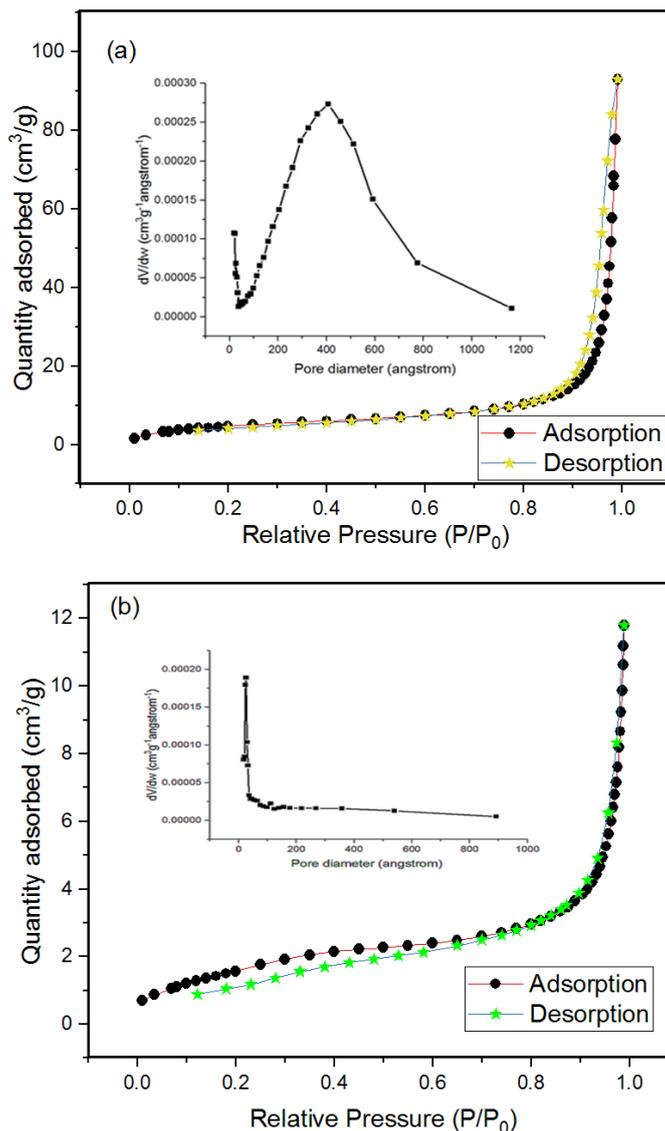
Figure 6: Isotherms of N_2 adsorption-desorption and BJH pore size distribution curves (insets) for (a) BiOI spheres and (b) BiOI plates.

3.2   Photocatalytic Activities of BiOI

3.2.1   Influence of Catalyst Morphology

BiOI spheres and BiOI plates have quite different morphologies, which is expected to result in difference of performance. This was confirmed by subjecting equal amounts of both BiOI spheres and BiOI plates to photocatalytic degradation of norfloxacin of similar concentrations, which is resistant to photolytic reactions as reported in literatures [41, 42]. As shown in Fig. 6, higher degradation efficiency was recorded by BiOI spheres as compared to BiOI plates, this was attributed to the high adsorption of norfloxacin onto the surface of BiOI spheres due to its mesoporous structure, resulting in enhanced photocatalytic activity.
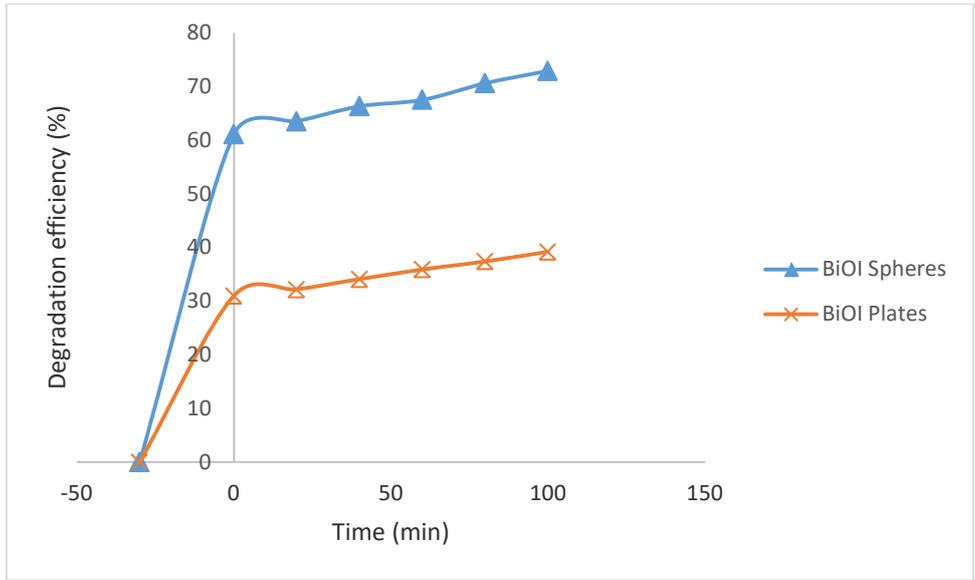
Figure7: Influence of BiOI morphology on the photodegradation of norfloxacin

3.2.2   Influence of Catalyst Dosage

At this stage, variable amounts of BiOI spheres (0.5 – 2 g/L) were used as photocatalysts for the degradation of norfloxacin solutions of the same concentration. As shown in Fig. 7, when catalyst dosage increases from 0.5 g/L to 1 g/L, degradation efficiency also increases. At 1 g/L, the optimum dosage was attained, and hence any further increase does not increase surface area but results in agglomeration of particles thereby increasing the turbidity of the solution which inturn blocks radiation, a paramount requirement for photodegradation [43].
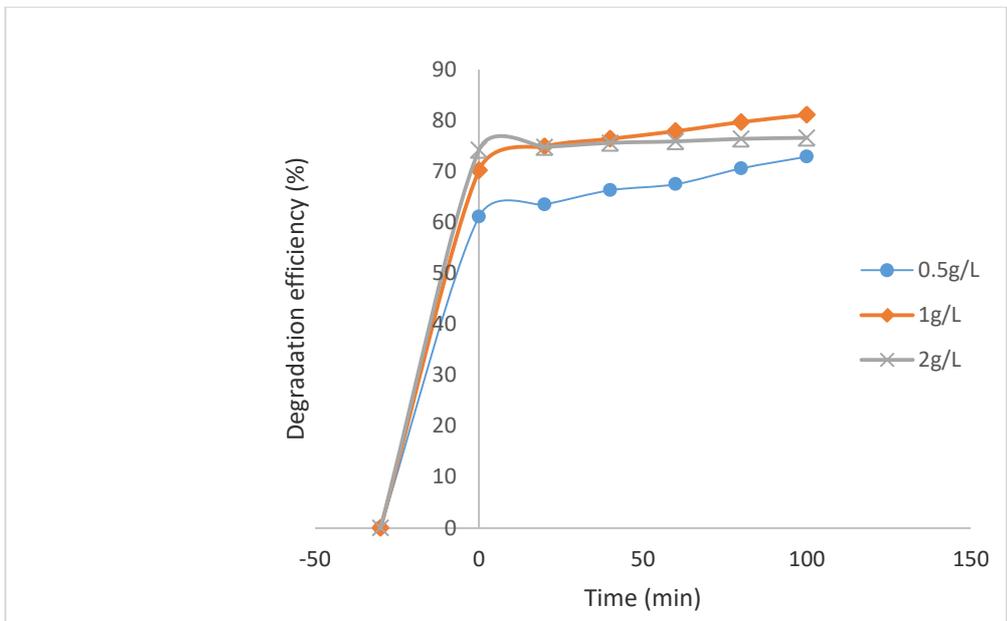

Figure 8: Influence of BiOI spheres dosage on the photodegradation of norfloxacin

3.2.3   Influence of Pollutant Concentration

This was studied by varying the norfloxacin concentration from 10 – 20 ppm at a catalyst loading of 1 g/L. It can be observed from Fig. 8, a high degradation efficiency was recorded at low concentration, but begins to decline with increase in concentration. An explanation to that is, as concentration increases, more reactive species (OH$^.$ and O$_2$$^{.-}$) are needed for the successful photodegradation of norfloxacin, which in this case keeps on decreasing with increase in concentration, due to fall down in the amount of light reaching BiOI. It is worth noting here that the insufficiency of reactive species (OH$^.$ and O$_2$$^{.-}$) resulted in continuous decrease of degradation efficiency with increase in concentration [44].
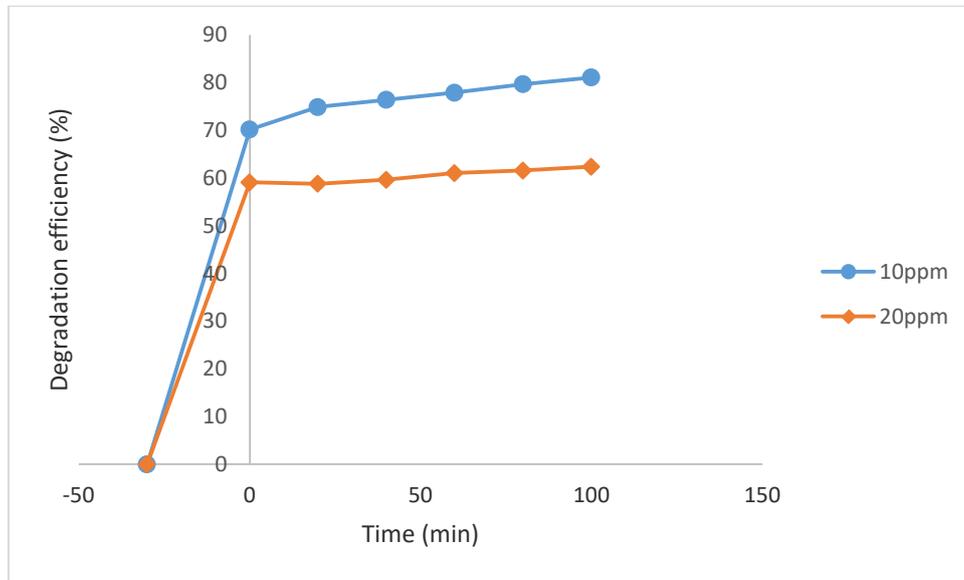

Figure 9: Influence of pollutant concentration on the photodegradation of norfloxacin

3.3   Reaction Mechanism

This process gets initiated when a photon of visible light having energy greater than the band gap of BiOI (i.e. hυ > 1.835 eV for BiOI spheres or hυ > 1.856 eV for BiOI plates) strikes its surface, electron then leaves the valence band (VB) thereby creating a hole (i.e. h$_{VB}$$^+$) and moves to the conduction band (CB) making it electron rich (i.e. e$^-$$_{CB}$).

$$BiOI + h\upsilon \text{ (visible)} \rightarrow BiOI\ (h_{VB}^+ + e_{CB}^-) \qquad (4)$$
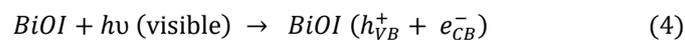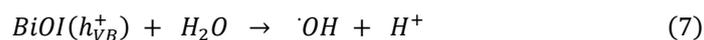
Electron in the conduction band converts the adsorbed oxygen on the surface of the photocatalyst to superoxide radical ($O_2^{.-}$).

$$BiOI(e_{CB}^-)\ +\ (O_2)_{ads}\ \rightarrow\ O_2^{.-} \qquad (5)$$
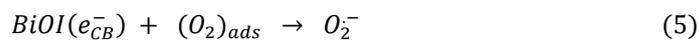
The hole in the valence band abstract an electron from the adsorbed water molecule or hydroxyl ions forming hydroxyl radicals.

$$BiOI(h_{VB}^+)\ +\ {}^-OH\ \rightarrow\ {}^.OH \qquad (6)$$

$$BiOI(h_{VB}^+) \ + \ H_2O \ \rightarrow \ ^{\cdot}OH \ + \ H^+ \tag{7}$$

The superoxide radical gets protonated, resulting in the formation of perhydroxyl radicals.

$$O_2^{\cdot-} \ + \ H^+ \ \rightarrow \ HO_2^{\cdot} \tag{8}$$

Subsequent step involves formation of hydrogen peroxide

$$BiOI(e_{CB}^-) \ + \ HO_2^{\cdot} \ + \ H^+ \ \rightarrow \ BiOI \ + \ H_2O_2 \tag{9}$$

This is the followed by the cleavage of hydrogen peroxide producing hydroxyl radicals

$$H_2O_2 \ + \ h\upsilon \rightarrow \ 2 \ ^{\cdot}OH \tag{10}$$

The final stage involves degradation of norfloxacin by hydroxyl radicals

$$^{\cdot}OH \ + \ Norfloxacin \ \rightarrow \ Degraded \ or \ mineralised \ products \tag{11}$$

4 Conclusion

In this study, both BiOI spheres and BiOI plates were successfully fabricated using low cost and eco-friendly room temperature solid-state synthesis method. Difference in morphology was achieved using PEG400, which due to its viscosity resulted in self-assembly of plates forming spheres. Although low concentration of norfloxacin was tested for photodegradation in the presence of both BiOI spheres and BiOI plates. Higher degradation efficiency was achieved using BiOI spheres as compared with BiOI plates. This is due to the morphology, surface area and pore volume of BiOI spheres, resulting in higher adsorption of norfloxacin, which is essential for decomposition. Moreover, the facile methods presented in this research can be adopted for the easy, fast and large scale synthesis of other bismuth-oxyhalides based photocatalysts.

References

[1]. Simoens, S., et al., Consumption patterns and in vitro resistance of Streptococcus pneumoniae to fluoroquinolones. Antimicrobial agents and chemotherapy, 2011. **55**(6): p. 3051-3053.

[2]. Hirsch, R., et al., Occurrence of antibiotics in the aquatic environment. Science of the Total Environment, 1999. **225**(1): p. 109-118.

[3]. Babić, S., M. Periša, and I. Škorić, Photolytic degradation of norfloxacin, enrofloxacin and ciprofloxacin in various aqueous media. Chemosphere, 2013. **91**(11): p. 1635-1642.

[4]. An, T., et al., Mechanistic considerations for the advanced oxidation treatment of fluoroquinolone pharmaceutical compounds using TiO2 heterogeneous catalysis. The Journal of Physical Chemistry A, 2010. **114**(7): p. 2569-2575.

[5]. Rigos, G., et al., Potential drug (oxytetracycline and oxolinic acid) pollution from Mediterranean sparid fish farms. Aquatic Toxicology, 2004. **69**(3): p. 281-288.

[6]. Prutthiwanasan, B., C. Phechkrajang, and L. Suntornsuk, Fluorescent labelling of ciprofloxacin and norfloxacin and its application for residues analysis in surface water. Talanta, 2016. **159**: p. 74-79.

[7]. Zorita, S., L. Mårtensson, and L. Mathiasson, Occurrence and removal of pharmaceuticals in a municipal sewage treatment system in the south of Sweden. Science of the total environment, 2009. **407**(8): p. 2760-2770.

[8]. Ferreira, V.R., et al., Fluoroquinolones biosorption onto microbial biomass: activated sludge and aerobic granular sludge. International Biodeterioration & Biodegradation, 2016. **110**: p. 53-60.

[9]. Ebrahimpour, B., Y. Yamini, and M. Moradi, Application of ionic surfactant as a carrier and emulsifier agent for the microextraction of fluoroquinolones. Journal of pharmaceutical and biomedical analysis, 2012. **66**: p. 264-270.

[10]. Zhu, L., et al., Electrochemical oxidation of fluoroquinolone antibiotics: Mechanism, residual antibacterial activity and toxicity change. Water research, 2016. **102**: p. 52-62.

[11]. Martín, M.B., et al., Degradation of alachlor and pyrimethanil by combined photo-Fenton and biological oxidation. Journal of hazardous materials, 2008. **155**(1): p. 342-349.

[12]. Murthy, H.R. and H. Manonmani, Aerobic degradation of technical hexachlorocyclohexane by a defined microbial consortium. Journal of hazardous materials, 2007. **149**(1): p. 18-25.

[13]. Ahmad, A., L. Tan, and S.A. Shukor, Dimethoate and atrazine retention from aqueous solution by nanofiltration membranes. Journal of hazardous materials, 2008. **151**(1): p. 71-77.

[14]. Maldonado, M., et al., Partial degradation of five pesticides and an industrial pollutant by ozonation in a pilot-plant scale reactor. Journal of hazardous materials, 2006. **138**(2): p. 363-369.

[15]. Saritha, P., et al., Comparison of various advanced oxidation processes for the degradation of 4-chloro-2 nitrophenol. Journal of Hazardous Materials, 2007. **149**(3): p. 609-614.

[16]. Kato, S., et al., Photocatalytic degradation of gaseous sulfur compounds by silver-deposited titanium dioxide. Applied Catalysis B: Environmental, 2005. **57**(2): p. 109-115.

[17]. Xu, Y., Comparative studies of the Fe 3+/2+–UV, H 2 O 2–UV, TiO 2–UV/vis systems for the decolorization of a textile dye X-3B in water. Chemosphere, 2001. **43**(8): p. 1103-1107.

[18]. Tokunaga, S., H. Kato, and A. Kudo, Selective preparation of monoclinic and tetragonal BiVO4 with scheelite structure and their photocatalytic properties. Chemistry of Materials, 2001. **13**(12): p. 4624-

4628.

[19]. Wu, T., et al., Bi 2 S 3 nanostructures: a new photocatalyst. Nano Research, 2010. **3**(5): p. 379-386.

[20]. Saison, T., et al., New insights into Bi2WO6 properties as a visible-light photocatalyst. The Journal of Physical Chemistry C, 2013. **117**(44): p. 22656-22666.

[21]. Zhang, L., et al., Sonochemical synthesis of nanocrystallite Bi 2 O 3 as a visible-light-driven photocatalyst. Applied Catalysis A: General, 2006. **308**: p. 105-110.

[22]. Yao, W.F., et al., Synthesis and photocatalytic property of bismuth titanate Bi 4 Ti 3 O 12. Materials Letters, 2003. **57**(13): p. 1899-1902.

[23]. Shimodaira, Y., et al., Photophysical properties and photocatalytic activities of bismuth molybdates under visible light irradiation. The Journal of Physical Chemistry B, 2006. **110**(36): p. 17790-17797.

[24]. Cao, X.-F., et al., Persimmon-like (BiO) 2 CO 3 microstructures: hydrothermal preparation, photocatalytic properties and their conversion into Bi 2 S 3. CrystEngComm, 2011. **13**(6): p. 1939-1945.

[25]. Chang, X., et al., BiOX (X= Cl, Br, I) photocatalysts prepared using NaBiO 3 as the Bi source: characterization and catalytic performance. Catalysis Communications, 2010. **11**(5): p. 460-464.

[26]. Shi, X., et al., Solvothermal synthesis of BiOI hierarchical spheres with homogeneous sizes and their high photocatalytic performance. Materials Letters, 2012. **68**: p. 296-299.

[27]. Cheng, H., B. Huang, and Y. Dai, Engineering BiOX (X= Cl, Br, I) nanostructures for highly efficient photocatalytic applications. Nanoscale, 2014. **6**(4): p. 2009-2026.

[28]. Cao, S., P. Zhou, and J. Yu, Recent advances in visible light Bi-based photocatalysts. Chinese Journal of Catalysis, 2014. **35**(7): p. 989-1007.

[29]. He, R., et al., 3D BiOI–GO composite with enhanced photocatalytic performance for phenol degradation under visible-light. Ceramics International, 2015. **41**(3): p. 3511-3517.

[30]. Han, S., et al., Fabrication of a β-Bi 2 O 3/BiOI heterojunction and its efficient photocatalysis for organic dye removal. Chinese Journal of Catalysis, 2015. **36**(12): p. 2119-2126.

[31]. Li, H., et al., Photocatalytic properties of BiOI synthesized by a simple hydrothermal process. Materials Letters, 2013. **107**: p. 262-264.

[32]. Ye, L., et al., BiOI thin film via chemical vapor transport: photocatalytic activity, durability, selectivity and mechanism. Applied Catalysis B: Environmental, 2013. **130**: p. 1-7.

[33]. Cao, Y., et al., Rapid one-step room-temperature solid-state synthesis and formation mechanism of ZnO nanorods as H 2 S-sensing materials. Solid-State Electronics, 2013. **82**: p. 67-71.

[34]. Xie, J., et al., Room-temperature solid-state synthesis of BiOCl hierarchical microspheres with nanoplates. Catalysis Communications, 2015. **69**: p. 34-38.

[35]. He, R., et al., Room-temperature synthesis of BiOI with tailorable (001) facets and enhanced photocatalytic activity. Journal of colloid and interface science, 2016. **478**: p. 201-208.

[36]. Gao, F., et al., Chemically bonded graphene/BiOCl nanocomposites as high-performance photocatalysts. Physical Chemistry Chemical Physics, 2012. **14**(30): p. 10572-10578.

[37]. Hu, Y.H., A highly efficient photocatalyst—hydrogenated black TiO2 for the photocatalytic splitting of water. Angewandte Chemie International Edition, 2012. **51**(50): p. 12410-12412.

[38]. Song, J.-M., et al., Hierarchical structured bismuth oxychlorides: self-assembly from nanoplates to nanoflowers via a solvothermal route and their photocatalytic properties. CrystEngComm, 2010. **12**(11): p. 3875-3881.

[39]. Jamil, T.S., E.S. Mansor, and R.A. Nasr, Degradation of Lindane using two nanosized BiOXs and their heterojunction under visible light. Desalination and Water Treatment, 2016. **57**(31): p. 14750-14761.

[40]. Xia, J., et al., Improved photocatalytic activity of few-layer Bi 4 O 5 I 2 nanosheets induced by efficient charge separation and lower valence position. Journal of Alloys and Compounds, 2017. **695**: p. 922-930.

[41]. Wang, J.-j., et al., Effect of bismuth tungstate with different hierarchical architectures on photocatalytic degradation of norfloxacin under visible light. Transactions of Nonferrous Metals Society of China, 2017. **27**(8): p. 1794-1803.

[42]. Li, J., et al., Fabrication of FeVO 4/Fe 2 TiO 5 composite catalyst and photocatalytic removal of norfloxacin. Chemical Engineering Journal, 2016. **298**: p. 300-308.

[43]. Sun, J., et al., Photocatalytic degradation of Orange G on nitrogen-doped TiO 2 catalysts under visible light and sunlight irradiation. Journal of hazardous materials, 2008. **155**(1): p. 312-319.

[44]. Bahnemann, W., M. Muneer, and M. Haque, Titanium dioxide-mediated photocatalysed degradation of few selected organic pollutants in aqueous suspensions. Catalysis Today, 2007. **124**(3): p. 133-148.